Hydrate stability and methane recovery from gas hydrate through CH4-CO2 replacement in different mass transfer scenarios

Pandey, Jyoti Shanker; von Solms, Nicolas

Published in:
Energies

Link to article, DOI:
10.3390/en12122309

Publication date:
2019

Document Version
Publisher's PDF, also known as Version of record

energies

MDPI

Article

Hydrate Stability and Methane Recovery from Gas Hydrate through CH_4–CO_2 Replacement in Different Mass Transfer Scenarios

Jyoti Shanker Pandey and Nicolas von Solms *

Center for Energy Resource Engineering (CERE), Department of Chemical Engineering, Technical University of Denmark, Lyngby 2800, Denmark; jyshp@kt.dtu.dk

* Correspondence: nvs@kt.dtu.dk

Received: 8 May 2019; Accepted: 11 June 2019; Published: 17 June 2019

Abstract: CH_4–CO_2 replacement is a carbon-negative, safer gas production technique to produce methane gas from natural gas hydrate reservoirs by injecting pure CO_2 or other gas mixtures containing CO_2. Laboratory-scale experiments show that this technique produces low methane volume and has a slow replacement rate due to the mass transfer barrier created due to impermeable CO_2 hydrate layer formation, thus making the process commercially unattractive. This mass-transfer barrier can be reduced through pressure reduction techniques and chemical techniques; however, very few studies have focused on depressurization-assisted and chemical-assisted CH_4–CO_2 replacement to lower mass-transfer barriers and there are many unknowns. In this work, we qualitatively and quantitatively investigated the effect of the pressure reduction and presence of a hydrate promoter on mixed hydrate stability, CH_4 recovery, and risk of water production during CH_4–CO_2 exchange. Exchange experiments were carried out using the 500 ppm sodium dodecyl sulfate (SDS) solution inside a high-pressure stirred reactor. Our results indicated that mixed hydrate stability and methane recovery depends on the degree of pressure reduction, type, and composition of injected gas. Final selection between CO_2 and CO_2 + N_2 gas depends on the tradeoff between mixed hydrate stability pressure and methane recovery. Hydrate morphology studies suggest that production of water during the CH_4–CO_2 exchange is a stochastic phenomenon that is dependent on many parameters.

Keywords: methane recovery; hydrate stability; CO_2 + N_2 injection; sodium dodecyl sulfate; mass transfer; morphology studies

1. Introduction

Methane hydrates are considered to be a potential source of clean energy. Gas hydrates are ice-like crystals, formed at low temperatures and in high-pressure conditions, having guest molecules of appropriate size and shape occupied inside water cages. Methane hydrate deposits are discovered in cold permafrost regions and deep ocean sediments [1] and are considered a potential source of methane gas production. Traditional production methods, e.g., depressurization, thermal stimulation, and chemical injection, are considered unsafe due to the perceived danger of hydrate dissociation causing geo-mechanical instability and natural disasters. Recently, a novel technique comprised of carbon dioxide (CO_2) or CO_2 + nitrogen (N_2) gas mixture injection into methane hydrate was proposed to produce methane gas and sequestration of CO_2 at the same time without disturbing the geo-mechanical stability [2]. This technology is still immature and there are many unknowns; for example, the reaction rate (kinetics), the stability of the mixed hydrates structures, structural changes, the recovery rate of methane, and the storage percentage of CO_2 are currently under investigation.

Results from laboratory-based experiments show different methane replacement percentages. Consistently lower methane recovery percentages have been attributed to the mass-transfer barrier

created on the outermost layer of methane hydrate due to the formation of CO_2 and mixed hydrates [3]. Yoon et al. [4] have further investigated this using Raman spectroscopy and concluded that contact between CH_4 hydrate and CO_2 molecules reduces over time due to a shielding effect caused by the outermost hydrate layer, which consists of the CO_2 hydrate that leads to rate decrease and the reaction to finally cease. Zhao et al. [5] have described methane CH_4–CO_2 replacement as a two-step process. The first step, described as a surface-replacement reaction between hydrate layer and injected CO_2 rich gas, creating a layer of mixed CH_4–CO_2 hydrate, lasts for very short time. The second step, a diffusion-driven reaction, is responsible for CO_2 molecule diffusion through methane hydrate and CO_2 hydrates and is considered as a rate-determining step. Many of the early studies on CH_4–CO_2 replacement dealt with bulk methane hydrate samples placed in contact with liquid or gaseous CO_2. McGrail et al. [6] have conducted the CH_4–CO_2 replacement in a high-pressure cell using powered CH_4 hydrate and found the replacement to be rapid during the first 200 min. In another experiment, Hauge et al. [7] calculated the CO_2 penetration rate into bulk hydrate as 0.55 mm/h at 2.5 °C. The probabilistic nature of the morphology of gas hydrate depends on many factors, such as apparatus design, experimental procedure, isolation of experimental setup from surroundings, impurities in the gas or bulk sample, and type and composition of injected gas [1].

Laboratory-scale experiments to investigate CH_4–CO_2 replacement reaction are long and tedious and start with the formation of artificial methane hydrate. Hydrate formation is a stochastic phenomenon and the onset of nucleation time to form hydrate depends on the method and the medium used; therefore, in general, they do not show reproducibility. Researchers have used different methods and media to form methane hydrate at a laboratory scale, including porous media, bulk water and a dispersed medium that results in a different mass-transfer scenario, different methane stability pressure, and growth kinetics. This initial difference in methane hydrate formation also affects the methane recovery potential during the CH_4–CO_2 replacement reaction. Methane hydrate and further CH_4–CO_2 replacement in bulk medium formation using bulk water is considered to be the most difficult and results in lower recovery due to the absence of a mineral surface [8]. Researchers added silica particles to accelerate the methane hydrate formation using bulk water. In this work, we used sodium dodecyl sulfate (SDS) in low concentrations to accelerate the methane hydrate formation; there is a necessity to study the effect of SDS on CH_4–CO_2 exchange under the chemical technique.

SDS is a well-known kinetic hydrate promoter that can enhance the hydrate formation rate both for CH_4 [9] and CO_2 hydrates [10]. It reduces hydrate nucleation induction time, enhances the hydrate growth rate, and maximizes the water-to-hydrate conversion efficiency [8] by creating the porous hydrate that allows for improved diffusion between liquid and gas and results in enhanced liquid-to-hydrate conversion. Thermal conductivity experiments of SDS-based methane hydrate formation also confirm the presence of porous gas hydrate as reflected by very low thermal conductivity [11]. SDS concentrations of 300–1000 ppm have been suggested as optimum concentrations to maximize the hydrate growth [12]. Higher concentrations above the optimal amount lead to excess foam formation that can be disadvantageous and need to be avoided. This can be done by using an antifoam agent along with SDS. SDS performance in the presence of an anti-foam agent has been studied by Pandey et al. [13]. It is suggested that SDS should be used in such low concentrations that it neither occupies the hydrate cages nor affects the temperature and pressure conditions of hydrate formation; hence, the presence of SDS is expected to not affect the driving force and thermodynamics between CH_4–CO_2 replacements. Research on SDS has mainly focused on hydrate promoters for potential applications in natural gas storage and transportation. Using SDS to form methane hydrate also increases the surface area compared to water [14]. Until now, only a few studies have focused on CH_4–CO_2 replacement in the presence of SDS. Zhou et al. [15,16] used SDS for hydrate formation in quartz sand and observed the enhanced replacement rate while injecting CO_2 emulsions. Using surfactants, such as SDS, may become a method for shortening methane hydrate formation and further studying the CH_4–CO_2 exchange in the presence of SDS could be advantageous to understand surfactant presence on CH_4–CO_2 exchange.

Depressurization is the most studied method to produce methane from gas hydrate deposits by reducing the pressure below its stability pressure, creating enhanced diffusion pathways and by dissociating the methane hydrates [17–20]. Depressurization or pressure drop is the pressure decrease induced by the field operator. It is considered an effective method, yet risky due to the risk of geo-mechanical instability and excess sand and water production. Controlled depressurization followed by CO_2-rich gas injection could act as a potential method to improve the mass transfer of CO_2 gas molecules by enhancing diffusion pathways inside the methane hydrate. The combined approach could have the potential to overcome an individual shortcoming in depressurization and CO_2 replacement. Studies based on temperature-assisted CH_4–CO_2 replacement have also been carried out [21,22]. Zhao et al. [23] studied the combined method using a high-pressure vessel and confirmed that the depressurization-assisted CH_4–CO_2 replacement produces higher methane percentages than the CO_2 replacement reaction. However, there are not enough studies currently available to understand the effect of different parameters, including the degree of pressure reduction, the risk of water production, the role of injected CO_2-rich gases in a combined method, the stability of mixed hydrates, and dominating mechanisms between depressurization and CO_2 replacement in a combined approach.

In this work, a high-pressure cell is used to form artificial methane hydrate using 500 ppm SDS solution to shorten the methane hydrate formation time and to improve the mass transfer process during CH_4–CO_2 exchange. To study the effect of the mechanical technique to improve mass transfer, immediate pressure reduction (IPR), followed by CO_2-rich gas injection using the huff-and-puff production technique is applied and a combined method of pressure reduction and CH_4–CO_2 replacement is applied. CH_4 recovery, mixed hydrate stability, and risk of water production are investigated. The key parameter varied is the amount of pressure reduction in the form of IPR, injection pressure, and CO_2 gas concentration in the CO_2-rich gas mixture. Additionally, the effect of an increase in SDS concentration on CH_4 recovery is studied. Change in morphology during the whole reaction is also recorded to investigate the risk of water produced during the process.

2. Materials and Methods

2.1. Setup and Materials

The combined method is studied using a stainless-steel hydrate pressure cell (HPC) with a fixed volume of 66.5 cm^3 and maximum working pressure of 200 bars. Visual inspection of gas hydrate formation is possible through two sapphire windows and used to record morphology variation during the replacement reaction. A safety valve is attached to the reactor. The reactor is connected to the gas supply vessel and the vacuum pump. A schematic layout of the experimental setup is shown in Figure 1. The HPC is connected with a cooling bath, data-acquisition setup, gas supply, and vacuum pump. It is possible to stir the reactor at high pressure and pictures are taken at regular intervals via web camera through a sapphire glass window. At the end of the experiment, a small sample is collected for further analysis using gas chromatography. The temperature inside the cell is controlled by a coolant circulating in a jacket surrounding the cell using a cooling bath. The pressure and temperature are monitored by using a pressure transducer sensor and a platinum resistance probe placed inside the cell, respectively, and recorded using data-acquisition software. Analytical-grade methane (99.99%), carbon dioxide (99.99%), and nitrogen (99.99%) are obtained from AGA Gas Company. Two different gas mixtures using CO_2 and N_2 gases with different CO_2 mole fractions (10% and 20% CO_2, respectively) and a Hewlett–Packard gas chromatograph (HP 7890) are used to analyze the composition of the gas mixture after the experiment. 500 ppm SDS solution is prepared using distilled water.

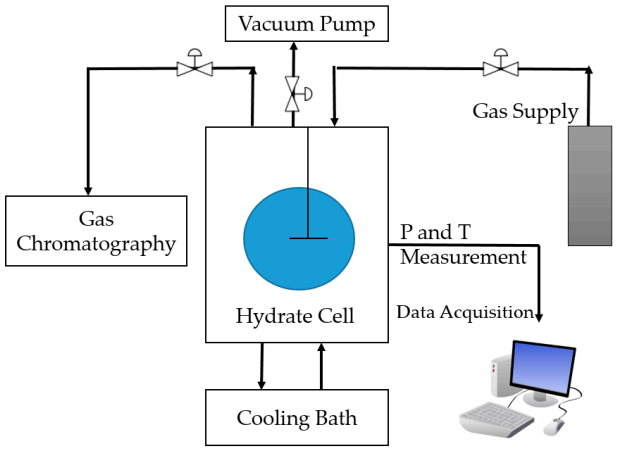

Figure 1. Schematic diagram of the high-pressure cell (HPC) used during the experiment. Initial Pressure and Temperature are 90 bars and 25 °C. Cooling is applied using cooling bath.

2.2. Procedure

Prior to the experiment, the reactor is cleaned with distilled water and ethanol. A stirring bar is placed in the cell, the cell lid is sealed, and the air inside is evacuated using a vacuum pump for 30 min. After the vacuum is established, the cell is loaded with 25 mL of 500 ppm SDS sample through a valve. After loading the sample, the HPC is pressurized with methane gas at 90–91 bars and 25 °C and the whole system is left to stabilize for some time. After stabilization, cooling is started and stirring equal to 450 rpm is set. Stirring is performed to increase the gas–liquid contact area to shorten the hydrate formation time. As cooling inside the reactor starts, hydrates begin to form when the experimental temperature goes below hydrate equilibrium temperature for a given initial operating pressure, such that the whole system reaches a sub-cooling state ($T_{exp} < T_{eq}$) [24]. Hydrate formation is identified by a sudden drop in pressure inside the HPC and, at this stage, stirring is stopped due to the presence of ice-like crystals inside the cell. The system is left for a few minutes to achieve pressure stabilization. Once pressure and temperature are stabilized, the methane gas inside is vented quickly and CO_2 gas or CO_2 + N_2 is injected at different pressures.

Figure 2 describes the different stages of the experiment. The first step is the formation of artificial methane hydrate using SDS solution. It is observed in the presence of SDS that methane hydrates are formed within 2–3 h and, after stirring is stopped, hydrates are allowed to stabilize for around 18–24 h. It is also observed that artificial methane hydrates are stabilized in the pressure range between 26–28 bars for temperatures of 1–1.5 °C. After that, methane gas is vented quickly and CO_2 + N_2 gas or CO_2 is injected quickly and the system is left idle for 72 h for replacement to take place.

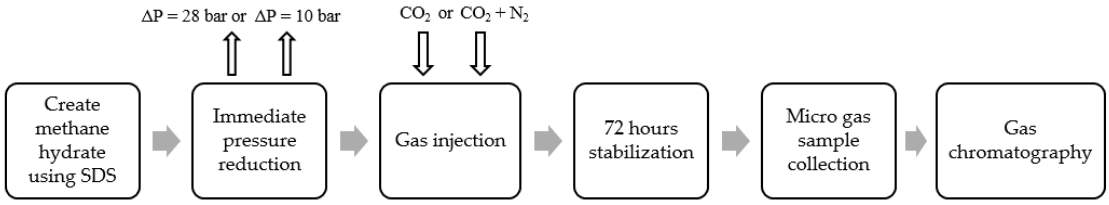

Figure 2. Experimental steps followed throughout the experiment.

Table 1 describes the breakdown of all experimental runs. All runs are divided into two sets, wherein a total of five runs are performed in set S1 and nine runs are performed in set S2. In the case of gas mixture CO_2 + N_2, the composition of CO_2 is increased from 10% to 20% on a mole basis. Sets S1 and S2 are defined based on the amount of IPR represented as a change in pressure, ΔP, applied before the injection of CO_2-rich gas. Under S1, ΔP = 28 bars and for S2, ΔP = 10 bars of pressure drop is applied. ΔP = 28 bars indicate the pressure inside the high-pressure cell reached atmospheric

pressure while ΔP = 10 bars means only a partial pressure drop occurred. IPR is achieved quickly and carefully within a few minutes. IPR is expected to act as a shock force to initiate cage breakage and create diffusion channels. During IPR, it is observed that, for ΔP = 10 bar, no water is observed during pressure reduction, whereas for ΔP = 28, a small amount of water is found coming from the venting valve, which supports the theory that, at a high-pressure reduction, cage breakage leads to hydrate dissociation and water and gas production. The higher the degree of cage breakage, the higher the chance that hydrate dissociation and release of water and gas occurs (common mechanism behind depressurization). Once IPR is applied, a different gas or gas mixture is injected inside the hydrate, as per details given in Table 1 and the system is left to stabilize for 72 h. During the 72 h of stabilization, pictures are collected at regular intervals, especially after 24, 48, and 72 h to record the change in morphology. After 72 h, the gas sample above the hydrate is collected for gas chromatography analysis to find out the gas composition.

Table 1. Experimental plan divided into two sets, S1 and S2, based on amount of pressure reduction. Additionally, number of experiments including type of each gas injected.

Set	Total Run	ΔP	CO_2 Injection	CO_2 (10%) +N_2 Injection	CO_2 (20%) + N_2 Injection
S1	5	28 bars	2	3	0
S2	9	10 bars	4	4	1

CO_2 and CO_2 + N_2 gas mixtures are injected at various injection pressure ranges between 8 bars to 43 bars both above and below the methane hydrate stability pressure of 28 bars at 1–2 °C. Venting methane partial pressure by IPR would cause microchannel creation and improve diffusivity. In runs such as this, it is easier to control pressure than temperature. Circone et al. [25] have discussed the effect of operating pressure on CH_4–CO_2 replacement using Raman Spectroscopy and suggested that, at a given CH_4 partial pressure, the replacement rate is positively influenced by operating pressure. Results of the experiment are evaluated mainly on three parameters: Mixed hydrate stability pressure, methane recovery efficiency, and change in morphology to detect the presence of water during the experiment. These results are thoroughly discussed in the results and conclusion section.

2.3. Experimental Data Processing

The total number of moles of CH_4 injected into the pressure cell is calculated as given below:

$$n_{CH_{4,T}} = \frac{P_1 V_1}{Z_1 R T_1} \tag{1}$$

P_1 is the initial operating pressure after methane gas injection into the high pressure cell at the start of the experiment. $V_I (V_I = V_T - V_L)$ is the available gas volume. V_T and V_L are the total cell volume and SDS solution volume (equal to 25 mL), respectively. T_1 is the temperature inside the cell that corresponds to P_1. A compressibility factor, Z_1, at a given pressure and temperature is calculated using the Benedict–Webb–Rubin–Starling equation of state and R is the universal gas constant, 8.314 J mol K^{-1}.

Assuming the process is a constant volume process, which means available gas volume, V_I, remains constant after methane hydrate formation and $n_{CH_{4,H}}$ is the moles of the methane in the gas phase after methane hydrate is formed, given by the equation

$$n_{CH_{4,H}} = \frac{P_{stability} V_1}{Z_2 R T_2} \tag{2}$$

where $P_{stability}$ is the pressure once methane hydrate is formed, T_2 is the temperature recorded corresponding to $P_{stability}$, and Z_2 is the compressibility factor corresponding to $P_{stability}$ and T_2. The change in total number of moles of methane, $\Delta n_{CH4,H}$, trapped in methane hydrate is given by

$$\Delta n_{CH4,H} = \frac{P_1 V_1}{Z_1 R T_1} - \frac{P_{stability} V_1}{Z_2 R T_2} \tag{3}$$

The mass of the consumed water in the methane hydrate formation, m_c, can be calculated as

$$m_c = \Delta n_{CH4,H} N_H M_H \tag{4}$$

Here, M_H is the molar mass of water and N_H is the hydration number. N_H is considered constant for methane hydrate formation with pressure 1.9 to 9.7 MPa and temperature 263 to 285 K. The average hydration number is CH_4-5.99 (±0.07) H_2O and we use 6.0 in our studies [4]. The density of hydrate is assumed to be 0.9 (gm/cm^3). Therefore, the volume of hydrate (cm^3) is calculated as

$$V_H = \frac{m_c}{0.9} \tag{5}$$

Hydrate saturation can be calculated as

$$S_H = \frac{V_H}{V_L} \tag{6}$$

where V_L is the initial volume of the SDS solution and is equal to 25 mL. Gas uptake is calculated as the ratio of number of moles of methane gas captured in hydrate divided by the initial moles of the SDS solution and is given as

$$n_{methane,uptake} = \frac{\Delta n_{CH4,H}}{n_{SDS}} \tag{7}$$

Additionally, the percentage of SDS solution consumed, C_{SDSH}%, is determined from the equation below:

$$C_{SDSH}\% = \frac{\Delta n_{CH_4,H} * N_{Hyd}}{n_{SDS}} \times 100 \tag{8}$$

New gas volume available for gas injection is given by

$$V_n = V_T - V_H - V_{L1} \tag{9}$$

where V_{L1} is the volume of the SDS solution not converted into hydrate and is given by $V_{L1} = V_L(1 - C_{SDSH}\%)$.

The moles of methane gas in the gas phase after applying IPR ΔP are given by

$$n_{CH_{4,IPR}} = \frac{P_3 V_n}{Z_3 R T_{IPR}} \tag{10}$$

where P_3 is the final pressure of methane gas inside the HPC after IPR and T_{IPR} is the temperature that corresponds to P_3. The number of moles of M_i (CO_2-rich gas, either pure CO_2 or CO_2 + N_2 mixture) injected into the pressure cell, is calculated as

$$n_{Mi,T} = \frac{P_{inj} V_n}{Z_{inj} R T_{inj}} \tag{11}$$

where P_{inj} is the pressure recorded by data logger at the time of injection. T_{inj} is the temperature recorded inside the cell corresponding to P_{inj} and Z_{inj}. After Injecting M_i, a replacement process is

assumed to have started. For simplicity, V_n is considered constant under a constant volume assumption. The total number of moles of the gas 72 h after the replacement starts is given as

$$n_{M,E} = \frac{P_f V_n}{Z_f R T_f} \tag{12}$$

where P_f is the final stability pressure of mixed hydrate at the end of the experiment recorded in the high-pressure cell and T_f is the temperature recorded corresponding to P_f. The moles of methane, carbon dioxide, and nitrogen in the collected gas sample at the end of the experiment $n_{CH_{4,E}}$, $n_{CO_{2,E}}$, and $n_{N_{2,E}}$ are calculated as

$$\begin{aligned} n_{CH_{4,E}} &= n_{M,E} \times y_{CH_{4,G}} \\ n_{CO_{2,E}} &= n_{M,E} \times y_{CO_{2,G}} \\ n_{N_{2,E}} &= n_{M,E} \times y_{N_{2,G}} \end{aligned} \tag{13}$$

where $y_{CH_{4,G}}$, $y_{CO_{2,G}}$, and $y_{N_{2,G}}$ are the mole fractions of methane, carbon dioxide, and nitrogen in the gas sample, respectively, determined by gas chromatograph. The moles of methane released from the hydrate phase, $n_{CH4,Re}$, is determined by

$$n_{CH4,Re} = n_{CH4,E} - n_{CH4,IPR} \tag{14}$$

where $n_{CH4,IPR}$ is the number of moles of methane gas after IPR and just before injection of CO_2-rich gas. The recovery efficiency of methane donated by the replacement ratio is given by

$$R_{CH_4} = \frac{n_{CH_4,Re}}{\Delta n_{CH_4,H}} \times 100\% \tag{15}$$

where $\Delta n_{CH_4,H}$ is the number of moles of methane stored in hydrate.

3. Results and Discussion

In this study, the combined technique is studied using immediate pressure reduction (IPR), followed by the injection of CO_2-enriched gas at various injection pressures. Injection and production using same well is the well-known huff-and-puff method. CO_2 injection and production from shale reservoirs using the huff-and-puff method have been studied extensively [26]. The current work is one of the first studies in which pressure reduction and the huff-and-puff technique combination have been used to study CH_4–CO_2 exchange. Different degrees of pressure reduction by mechanical means stand to improve diffusion channels during the CH_4–CO_2 exchange. For chemical improvement, methane hydrate is formed using different SDS concentrations and CH_4–CO_2 exchange has been studied while keeping other parameters constant. Both qualitative and quantitative analyses are performed to study the effect of different degrees of IPR, type of gas injection on the stability of mixed gas hydrates, methane recovery efficiency, and risk of water production. There are a total of 14 experimental runs and progress that can be explained in five different steps, M_1–M_5, as highlighted in Table 2. Step M_1 includes SDS nucleation, which refers to the first microscopic detection of hydrate formation. Nucleation starts after methane dissolves into the bulk SDS solution. Step M_2 is about the rapid hydrate formation period. Hydrate nucleation and growth theories have been discussed elsewhere [27]. Step M_3 describes the period of stabilization where pressure and temperature achieve constant values within certain hours. In our experiments, it is evident from the results that $M_1 + M_2$ last for 2–6 h, consistently. This period is dependent on the operating pressure. The higher the operating pressure, the higher the driving force and the shorter the hydrate formation period [27]. Sub-cooling (ΔT) is the most often used term to define the driving force for hydrate formation and is given by the formula $\Delta T = T_{eq} - T_{exp}$, where T_{eq} is the equilibrium temperature and T_{exp} is the experimental temperature, such that $T_{exp} < T_{eq}$. Presence of SDS provides the certainty within the hydrate formation period, showing reproducibility in terms of achieving the final methane hydrate stability pressure and creating similar initial conditions before IPR

implementation. Further, the total time for $M_1 + M_2 + M_3$ is approximately 18–24 h. Stage M_4 includes IPR followed by gas injection. The total duration for IPR and gas injection lasts for a few minutes. Stage M_5 lasts for approximately 72 h to allow CH_4–CO_2 replacement.

Table 2. Summary of experimental steps.

STEP M_1	Hydrate nucleation
STEP M_2	Hydrate growth
STEP M_3	Hydrate stability acquired
STEP M_4	Instant pressure reduction step followed by gas injection
STEP M_5	Replacement reaction for 72 h

Table 3 summarizes the methane hydrate formation in the presence of SDS in all 14 experimental runs. Methane hydrate saturation varies from 58–61% and water conversion to hydrate (C_{wh}%) varies from 52–55%. $P_{stability}$ is the methane hydrate stability pressure at the end of $M_1 + M_2 + M_3$. P_1 is the initial operating methane pressure, $P_{stability}$ is the pressure inside cell after methane hydrate formation, and $n_{CH4,\,H}$ is the moles of methane trapped in hydrate. C_{SDSH}% is the percentage of SDS solution converted into methane hydrate. Based on IPR, runs 1–5 are in set S1 and runs 6–14 are in set S2, as previously shown in Table 3.

Table 3. Sodium dodecyl sulfate (SDS)-based methane hydrate formation in all experimental runs (methane hydrate formed using SDS concentration 500 ppm, ** for run 9 and 10, methane hydrate is formed using 2000 and 3000 ppm SDS solution).

Run#	P_1 (bars)	$P_{stability}$ (bars)	$\Delta n_{CH4,\,H}$ (m moles)	Hydrate Saturation	C_{SDSH}%	Methane Uptake (10^{-2})	IPR Applied (bars)
1	90.50	28.50	121.73	58%	52%	8.76	ΔP = 28
2	90.35	27.80	122.87	59%	53%	8.85	ΔP = 28
3	91.10	29.60	120.60	58%	52%	8.68	ΔP = 28
4	90.54	28.52	121.71	58%	52%	8.76	ΔP = 28
5	90.77	27.80	123.62	59%	53%	8.90	ΔP = 28
6	89.94	26.48	124.71	60%	53%	8.98	ΔP = 10
7	90.94	27.10	125.53	60%	54%	9.04	ΔP = 10
8	90.75	27.32	124.65	60%	54%	8.98	ΔP = 10
9 **	90.68	27.32	123.87	60%	53%	8.92	ΔP = 10
10 **	90.42	27.62	123.97	60%	53%	8.93	ΔP = 10
11	91.10	27.49	125.04	60%	54%	9.00	ΔP = 10
12	91.61	26.92	127.50	61%	55%	9.18	ΔP = 10
13	91.65	28.66	123.78	59%	53%	8.91	ΔP = 10
14	90.71	27.23	124.75	60%	54%	8.98	ΔP = 10

Figure 3 describes the P–T variation up to 10 h for two runs, #3 and #13. Run #3 is from set S1 and run #13 is from set S2. Run #3 has a longer nucleation time compared to run #13. This could be due to the presence of air with methane inside the high-pressure cell. With the rest of the runs, we achieve nucleation within 2 h consistently.

Figure 4 describes the M_4 and M_5 steps in set S1 and set S2. To differentiate S1 from S2, experiments are put in different timelines but with similar initial conditions before IPR is applied. In set S1, which includes runs 1–5, methane gas above methane hydrate vented quickly before injecting CO_2-rich gas at different injection pressures. State M_5 after injecting corresponds to an exchange between CH_4–CO_2 and leads to stabilization of pressure within 72 h. During M_4 in set S1, water production is observed while venting out the gas, which suggests that pressure reduction leads to dissociation of the hydrate and thus release of gas and water. Run #3 in set S1 corresponds to injection of $CO_2 + N_2$ gas mixture; therefore, during the replacement, mixed hydrate stability pressure moves to a higher value compared to initial methane hydrate stability pressure and suggests that replacement took place.

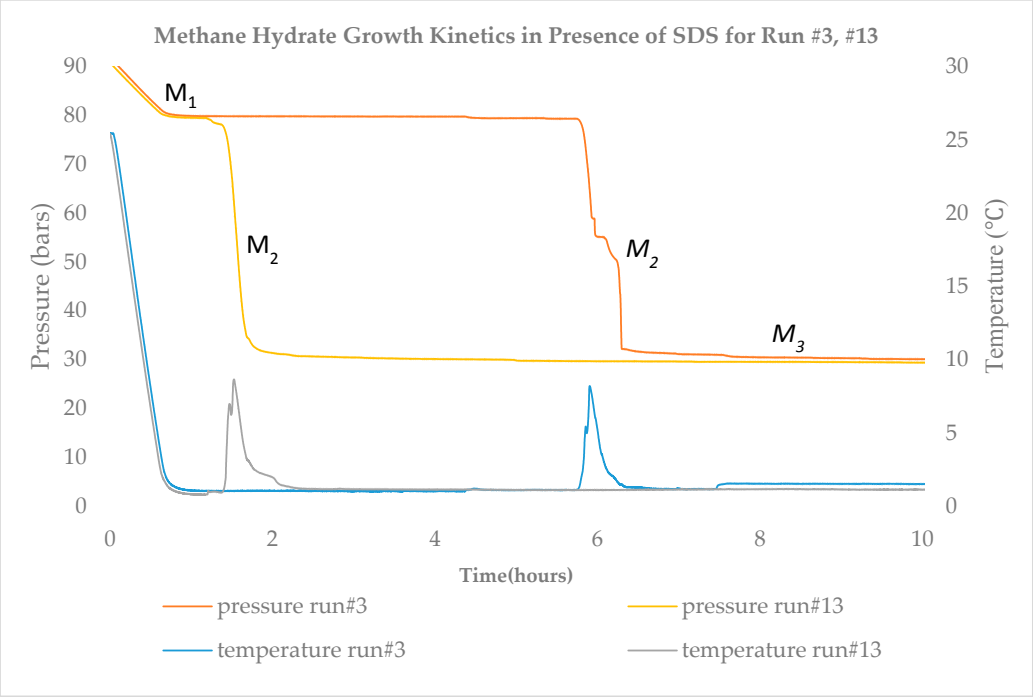

Figure 3. P–T readings for experiment run #3 from set S1 and run #13 from set S2 corresponding to methane hydrate growth kinetics in the presence of SDS.

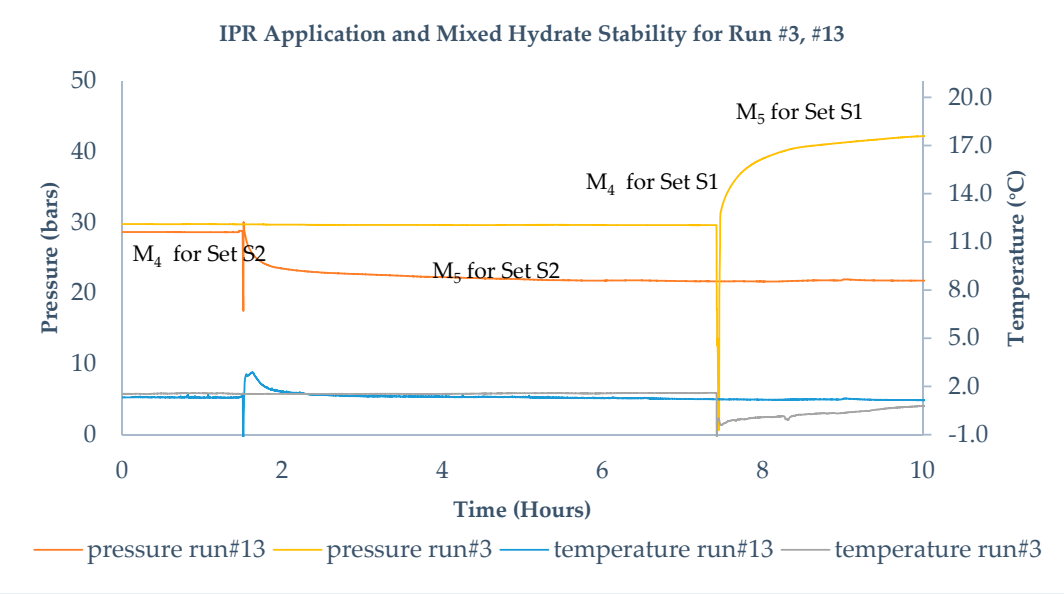

Figure 4. P–T readings for experiment run #3 from set S1 and run #13 from set S2 corresponding to IPR application and mixed hydrate stability pressure.

Run #13 is from set S2 and corresponds to IPR equal to about 10 bars followed by injection of CO_2 gas. CO_2 injection leads to a lower stability pressure than the methane hydrate pressure, which indicates that replacement took place. This is reflected as M_4 for set S2 and M_5 in Figure 4. IPR under set S2 leads to the breaking of hydrogen bonds between water molecules forming the cages, moving methane hydrate into a metastable state. It does not produce water, as observed during the venting out of methane before CO_2 injection, whereas a higher degree of IPR under set S1 initiates dissociation and is responsible for the production of water. Two different IPRs lead to two states of methane hydrate before the injection of CO_2 _rich gas. For IPR in S1, dissociation dominates, while for IPR in S2, the

metastable state and breaking of hydrogen bonds dominates. IPR is believed to improve the sample permeability and add additional diffusion channels, supporting the enhanced mass transfer for CO_2 molecules [19] and could be considered as a mechanical means to improve diffusion channels.

3.1. SDS-Based Methane Hydrate Formation

The summary based on Kumar et al. [12] suggests that SDS is one of the best hydrate promoters in the surfactant category and its performance can be further enhanced if mixed with another chemical, such as tetrahydrofuran (THF). SDS has distinctive two-stage growth kinetics differentiated by a sudden spike in temperature, as shown in Figure 3. The sharp temperature rise indicates the two distinct hydrate growth phases with a short duration in the first stage, followed by a significantly faster rate of hydrate formation in the second stage. In general, gas hydrate formation kinetics are very probabilistic and dependent on factors such as apparatus design, experimental procedure, reactor wall, driving force, and impurities in the sample [1].

Ganji et al. [28] have compared different surfactants on methane hydrate formation rate, stability, and storage capacity. Application of SDS for methane hydrate formation would lead to certainty in the hydrate formation without affecting the thermodynamics of methane hydrate. Due to the presence of SDS in the system, similar initial conditions have been achieved in all 14 runs before the instant pressure reduction.

Linga et al. [29] suggested that nucleation and growth of the hydrate are not only dependent on the operating pressure and concentration of the hydrate promoter but also on the design of the reactor. The authors of this paper believe that reactor design also influences the methane recovery as a wide range of methane recovery percentages are reported using bulk media with the HPC in literature.

3.2. Mixed Hydrate Stability Pressure

Table 4 summarizes the mixed hydrate stability pressure in all experimental runs in both sets. P_3 is the pressure after IPR applied, P_{inj} is the injection pressure of CO_2 rich gas, and P_f is the pressure recorded at the end of replacement reaction which corresponds to mixed hydrate stability pressure. Hydrate stability pressure is an indicator of thermodynamic stability achieved by a hydrate at a given temperature. Hydrate replacement experiments are performed at constant temperature conditions in which, before and after gas injection, hydrate stability pressure changes due to a replacement reaction. Therefore, it is a matter of interest for us to understand whether CO_2 and CO_2 + N_2 gas injection can lead to higher or lower stability pressures than the methane hydrate stability pressure.

Table 4. Experimental conditions including type and composition of gas injected, injection pressure P_{inj}, and mixed hydrate stability pressure P_f. Runs 1–5 are from set S1 and runs 6–14 are from set S2. To form methane hydrate, SDS 500 ppm concentration is used (except ** run 9 and 10, methane hydrate is formed using 2000 and 3000 ppm SDS solution).

Run#	$P_{stability}$ (bars)	IPR (bars)	P_3 (bars)	Gas Type	P_{inj} (bars)	P_f (bars)
1	28.50	ΔP = 28	0.3	CO_2 (10%) + N_2 (90%)	8.1	30.7
2	27.80	ΔP = 28	0.9	CO_2 (10%) + N_2 (90%)	20.9	30.5
3	29.60	ΔP = 28	0.6	CO_2 (10%) + N_2 (90%)	30.6	43.8
4	28.52	ΔP = 28	0.6	CO_2	43.1	37.9
5	27.80	ΔP = 28	0.5	CO_2	39.2	37.3
6	26.48	ΔP = 10	16.6	CO_2 (20%) + N_2 (90%)	29.06	25.00
7	27.10	ΔP = 10	18.2	CO_2 (10%) + N_2 (90%)	21.55	26.20
8	27.32	ΔP = 10	18.3	CO_2 (10%) + N_2 (90%)	30.42	34.59
9 **	27.32	ΔP = 10	16.4	CO_2 (10%) + N_2 (90%)	29.10	30.80
10 **	27.62	ΔP = 10	18.9	CO_2 (10%) + N_2 (90%)	29.40	34.30
11	27.49	ΔP = 10	15.1	CO_2	30.20	22.00
12	26.92	ΔP = 10	15.5	CO_2	21.19	18.70
13	28.66	ΔP = 10	17.5	CO_2	30.09	23.17
14	27.23	ΔP = 10	17.6	CO_2	27.41	21.76

Figures 5 and 6 show the mixed hydrate stability in sets S1 and S2 after injecting CO_2-rich gases at different injection pressures.

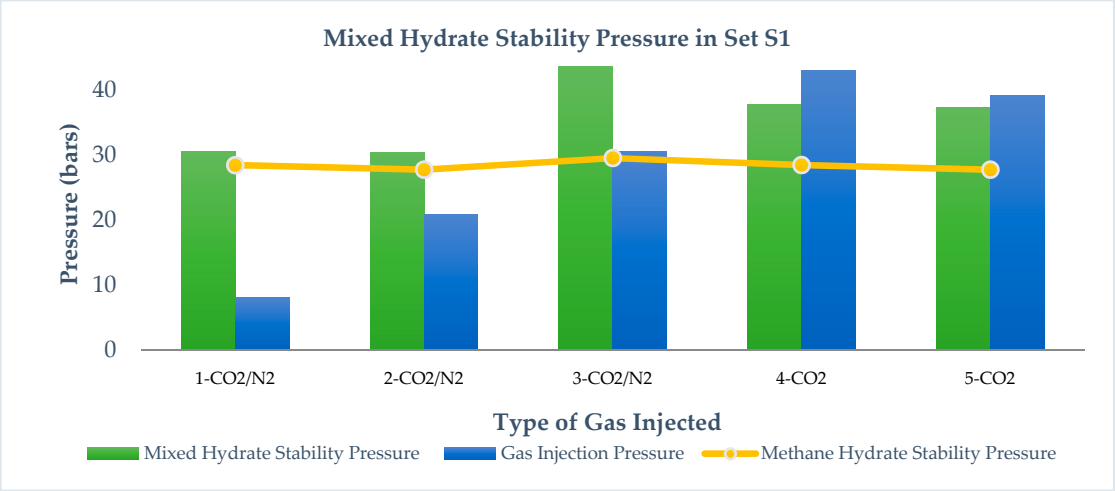

Figure 5. Mixed hydrate stability pressure after applying ΔP = 28 bars (set S1) and injecting different CO_2 and CO_2 + N_2 mixture at different injection pressures.

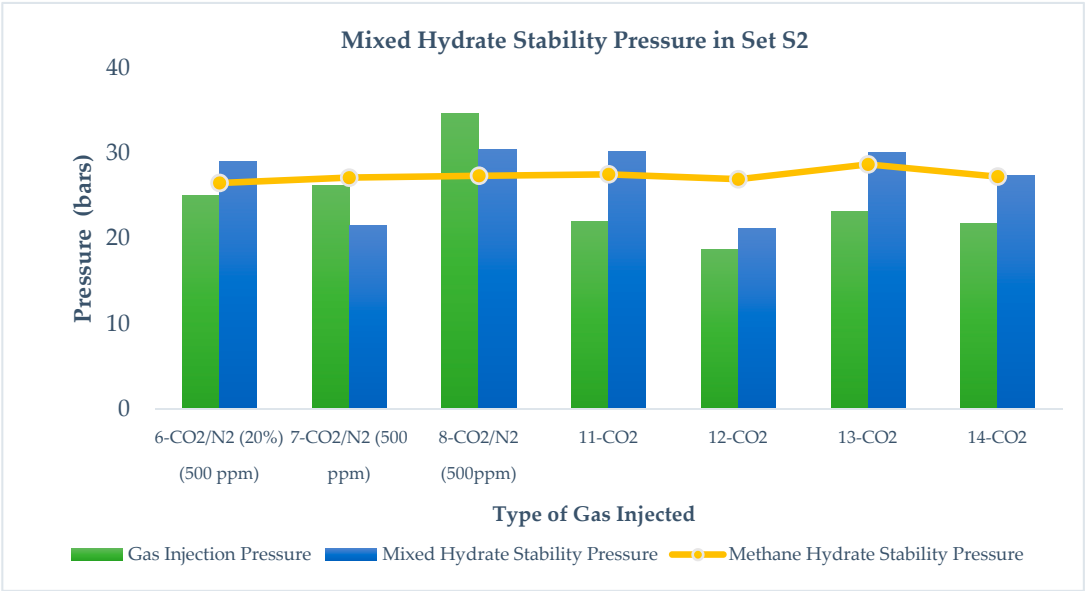

Figure 6. Mixed hydrate stability pressure after applying ΔP = 10 bars (Set S2) and injecting CO_2 and CO_2 + N_2 mixture at different injection pressures.

From runs 1, 2, and 3 in set S1 and runs 7 and 8 in set S2, we observe that P_f (mixed hydrate) > $P_{Injection}$ (CO_2 + N_2), whereas in runs 4 and 5 in set S1 and runs 11, 12, 13, and 14 in set S2, P_f (mixed hydrates) < $P_{Injection}$ (CO_2). It is evident from the results that CO_2 injection leads to lower stability pressure than gas injection pressure, while CO_2 + N_2 injection leads to higher mixed hydrate pressure than injection pressure. P_{inj} is pressure induced by injecting CO_2-rich gases while P_f is the measured pressure after the replacement reaction. This relationship is independent of pressure reduction in S1 and S2 as well as the range of pressure injection below and above the methane stability pressure. This is because the mixed hydrate stability pressure is mostly affected by the injected gas thermodynamics and its difference in methane hydrate thermodynamics. Addition of N_2 into the CO_2 leads to higher stability pressure of the gas mixture because N_2 converts into hydrate at a higher pressure and thus the thermodynamic force between CH_4 and CO_2 reduces due to the presence of N_2 in CO_2. Run 6 in S2

shows that, by increasing CO_2 content in the gas mixture, a lower stability pressure can be achieved than the injected gas pressure. Even at the same injection pressure in runs 8 and 11 in S2, CO_2 leads to a more stable hydrate pressure compared to $CO_2 + N_2$.

Comparing runs 11, 12, 13, and 14 in S2, it is also observed that $P_{f\ mixed\ hydrate}$ (after CO_2 injection) < P_{CH4} (independent of a range of injection pressure), which means in S2, CO_2 injection leads to a more stable hydrate than methane hydrate. However, a similar observation is not found valid after $CO_2 + N_2$ injection.

For set S1 in Figure 7, correlation between mixed hydrate stability pressure P_f, and gas injection pressure P_{inj}, is not very clear, However, in set S2, as shown in Figure 8, there exists a correlation between mixed hydrate stability pressure, P_f, and gas injection pressure, P_{inj}, that is independent of the type of gas injection and amount of immediate pressure reduction.

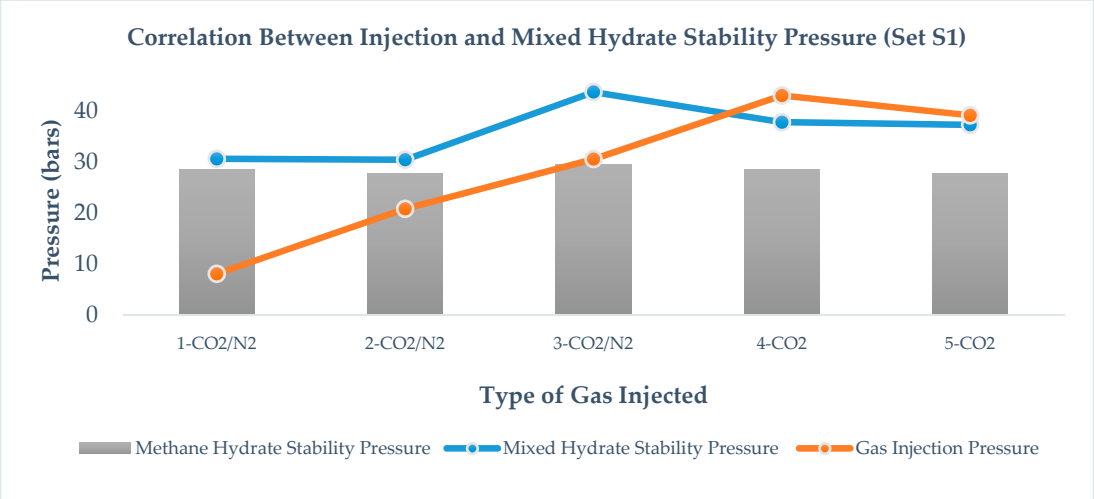

Figure 7. Correlation between mixed hydrate pressure and gas injection pressure for set S1.

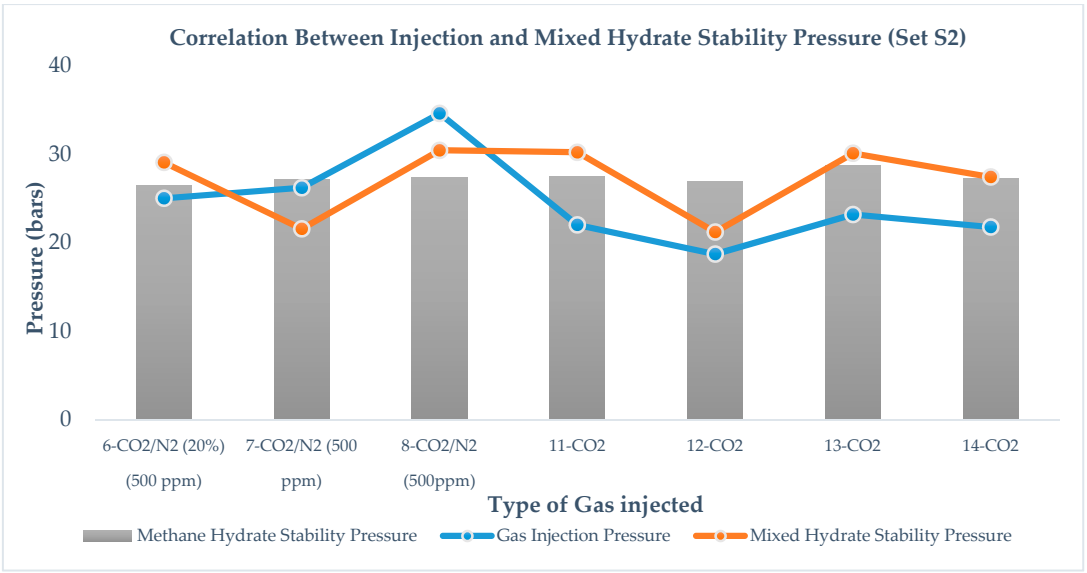

Figure 8. Correlation between mixed hydrate pressure and gas injection pressure for set S2.

Based on the above results, it can be concluded that CO_2 injection is the better option compared to $CO_2 + N_2$ gas injection because it leads to a more stable hydrate than $CO_2 + N_2$. This is reflected by a lower stability pressure at the end of experiment. In the case of CO_2 injection, mixed hydrate stability pressure is recorded as lower than the injection pressure. It can be derived that, to achieve

higher stability during the replacement reaction, the CO_2 injection pressure should be lower than the methane hydrate stability pressure. In the case of injection of the CO_2 + N_2 mixture, to achieve a lower pressure than gas injection, a higher CO_2 content in the gas mixture is recommended. Tsypkin [30] concluded that an increase in injection pressure might lead to termination of the replacement reaction due to suppression of methane hydrate dissociation.

3.3. Methane Recovery Efficiency

Another major factor of concern during methane production through gas injection is methane-recovery efficiency. In this study, we are interested to know the effect of ΔP, the effect of injection gas, and the effect of injection pressure on the methane-recovery efficiency. Methane-recovery efficiency is calculated as the ratio of number of moles of CH_4 released to the number of moles of CH_4 in the hydrates. Moles of CH_4 hydrates are considered at the end of CH_4 hydrate formation. Table 5 summarizes the methane-recovery efficiency in all experimental runs. $\Delta n_{CH4,H}$ is the number of moles of methane stored in hydrates and $nCH_{4,\,Re}$ is the number of moles of the methane recovery at the end of the run, measured using gas chromatograph. Figures 9 and 10 summarize the results of methane recovery efficiency for sets S1 and S2.

Table 5. Methane-recovery efficiency calculation for runs 1–5 in set S1 and runs 6–14 in set S2 (** for runs 9 and 10, methane hydrate is formed using 2000 and 3000 ppm SDS solution). P_{inj} is the injection pressure of CO_2-rich gas injected. RCH_4% is the methane-recovery efficiency.

Run#	$P_{stability}$ (bars)	IPR (bars)	Gas Type	P_{inj} (bars)	$\Delta n_{CH4,H}$ (m moles)	$n_{CH4,\,Re}$ (m moles)	R_{CH4}%
1	28.50	ΔP = 28	CO_2 (10%) + N_2 (90%)	8.1	121.73	49.81	41%
2	27.80	ΔP = 28	CO_2 (10%) + N_2 (90%)	20.9	122.87	36.75	30%
3	29.60	ΔP = 28	CO_2 (10%) + N_2 (90%)	30.6	120.60	45.57	38%
4	28.52	ΔP = 28	CO_2	43.1	121.71	4.996	4%
5	27.80	ΔP = 28	CO_2	39.2	123.62	5.449	4%
6	26.48	ΔP = 10	CO_2 (20%) + N_2 (90%)	29.06	124.71	11.36	9%
7	27.10	ΔP = 10	CO_2 (10%) + N_2 (90%)	21.55	125.53	11.43	9%
8	27.32	ΔP = 10	CO_2 (10%) + N_2 (90%)	30.42	124.65	12.36	10%
9 **	27.32	ΔP = 10	CO_2 (10%) + N_2 (90%)	29.10	123.87	9.88	8%
10 **	27.62	ΔP = 10	CO_2 (10%) + N_2 (90%)	29.40	123.97	15.62	13%
11	27.49	ΔP = 10	CO_2	30.20	125.04	6.56	5%
12	26.92	ΔP = 10	CO_2	21.19	127.50	3.40	3%
13	28.66	ΔP = 10	CO_2	30.09	123.78	5.36	4%
14	27.23	ΔP = 10	CO_2	27.41	124.75	2.91	2%

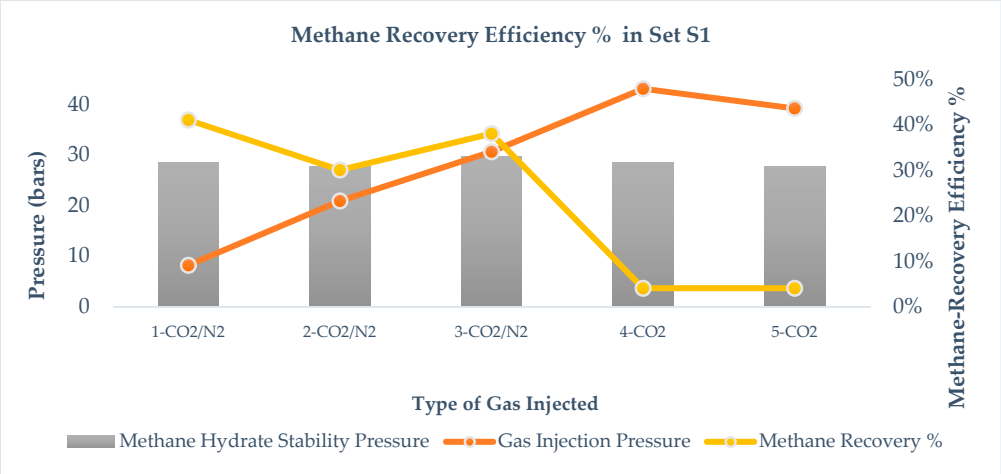

Figure 9. Methane-recovery efficiency after applying ΔP = 28 bars (set S1) and injecting CO_2 and CO_2 + N_2 mixture at different injection pressures.

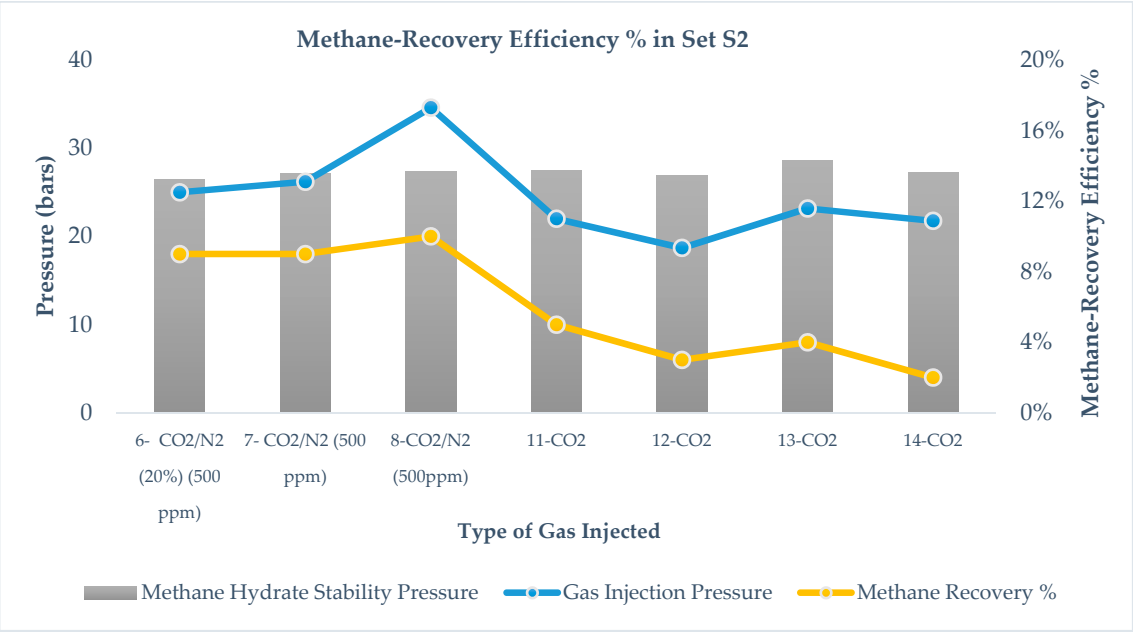

Figure 10. Methane-recovery efficiency after applying ΔP = 10 bars (set S2) and injecting CO_2 and CO_2 + N_2 mixture at different injection pressures.

Figures 9 and 10 Showcase the difference in methane recovery for CO_2 + N_2 and CO_2 gas in set S1 and set S2. For set S1 in Figure 9, during runs 1–3, it shows that the CO_2 + N_2 gas mixture leads to 30–40% gas recovery, whereas during runs 4 and 5, CO_2 leads to 5% gas recovery. For set S2 in Figure 10, during runs 7 and 8, CO_2 + N_2 gas mixture leads to 10% methane recovery, whereas during runs 11–14, CO_2 leads to very low recovery, <5%. Koh et al. [31], in their review paper, summarized the methane-recovery yield reported elsewhere. Comparison of results show that methane recovery from CO_2 + N_2 injection has a consistently higher methane recovery from pure CO_2 injection. Therefore, it can be derived that the CO_2 + N_2 gas mixture leads to higher gas recovery than pure CO_2, independent of degree of pressure reduction. This difference is due to N_2-assisted higher dissociation and water generation which is re-converted into CO_2. However, methane could not reconvert into methane hydrate and could not reoccupy cages due to the presence of N_2. In the case of CO_2, methane was reconverted into methane hydrate and a layer of CH_4–CO_2 was generated, which stopped additional methane recovery. It can be derived from the results that the degree of pressure reduction plays an important role in methane recovery if the CO_2 + N_2 gas mixture is injected. The effect of pressure reduction is negligible in the case of CO_2 injection and no substantial change in methane recovery between S1 and S2 is observed.

Chen et al. [32] have studied the effect of injection pressure of CO_2 gas on replacement efficiency and suggested that lower injection pressure leads to dissociation of methane hydrate and that higher injection pressure would lead to accelerating CO_2 formation. However, a change in injection pressure does not show a strong influence on replacement efficiency. In our work, we do not see any trend between gas injection pressure and methane recovery for set S1, as shown in Figure 7 but for set S2, as shown in Figure 8 methane-recovery efficiency and gas injection pressure are correlated; however, no systematic correlation could be proposed at this point. From the results, we observed the pattern that, in the case of CO_2 + N_2 gas injection, recovery is consistently higher when the injection pressure of the gas mixture is close to or below the methane hydrate stability pressure, thus supporting Chen et al.'s experimental conclusions that a lower injection pressure below methane hydrate stability pressure would accelerate the dissociation of methane hydrate, while a higher injection pressure could lead to faster CO_2 hydrate formation, faster CH_4–CO_2 hydrate layer formation, and lower CH_4 recovery.

Run #6 in set S2 suggests that the CO_2 + N_2 mixture (20% CO_2) leads to equal methane recovery while creating more stable mixed hydrate if injected close to the initial methane hydrate stability pressure. Thus, a higher mole percentage of CO_2 is advantageous in a CO_2-rich gas mixture for improved methane recovery and higher stability of mixed hydrates.

3.4. Effect of SDS Concentration on Methane Recovery and Stability

As SDS concentration increases from 500 ppm to 2000 ppm, we observe an increase in methane recovery efficiency. Comparing runs 8–10, it is found that, between runs 8 and 9, methane recovery and methane stability improve, while from runs 9 to 10, methane recovery and instability decrease, as per Figure 11. At a higher concentration of 3000 ppm, methane-recovery efficiency and mixed hydrate stability decrease, because a higher surfactant concentration may lead to foam generation that may have created a barrier for effective CH_4–CO_2 replacement. It is also clear from Figure 11 that SDS does not disturb the methane hydrate stability pressure, as most of the methane hydrate stability pressure is in a small range (26–28 bars) when the temperature is between 1–2 °C, thus confirming that SDS is a kinetic hydrate promoter. Increasing the concentration in SDS does not lead to drastic change in methane recovery, which confirms that SDS does not affect the thermodynamics of CH_4–CO_2 replacement. Since SDS creates pseudo-porous media and accelerates the methane hydrate formation, use of SDS in low concentrations to form methane hydrate could be advantageous in reducing total experiment time. In the case of a higher concentration, to avoid the formation of foam, use of antifoam agent is recommended.

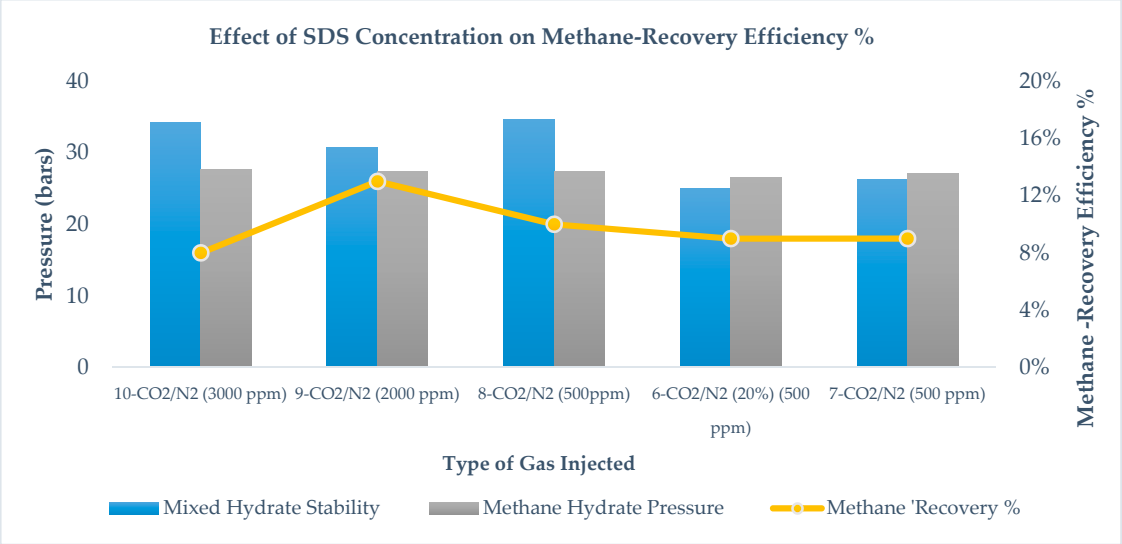

Figure 11. Effect of SDS concentration on methane-recovery efficiency in set S2.

3.5. Morphology Studies of Hydrate during the CO_2 and CO_2 + N_2 Injections

There are different theories proposed to explain the exact mechanism behind CH_4–CO_2 replacement. According to the first theory, CH_4–CO_2 replacement includes methane hydrate decomposition and reformation in the presence of CO_2-rich gas driven by the chemical potential gradient between gases and the hydrate phase. According to the second theory, CH_4–CO_2 replacement happens without any cavity destruction as no water was detected using magnetic resonance imagining (MRI) and differential scanning calorimeter (DSC) experiments. Therefore, it would be helpful to use an HPC to observe whether water is present during the replacement reaction. Figure 12 shows the typical gas hydrate morphology change during the experiment and highlights the interesting observation about change in morphology from a semi-solid hydrate to a crystal hydrate in a 24–72 h timeline, which occurs at the stage of CH_4–CO_2 exchange at constant temperature. It indicates a change in the water–gas contact

area during the replacement and improvement in the contact area leads to faster crystallization over a longer period.

Figure 12. Change in morphology in gas hydrate before and after the gas injection. Picture 3, 4, and 5 are after injection of CO_2-rich gases. Picture also shows the porous methane hydrate morphology in the presence of SDS. Picture 2 shows the morphology of methane hydrate during the IPR and subsequent gas injection.

Table 6 summarizes the morphology studies collected at the end of all experimental runs. Morphology observed is divided into two categories: Hydrate crystals and hydrate slurry. Crystal morphology is considered in those cases in which an ice-like structure is observed, while hydrate slurry is considered in those cases where the liquid state coexists with hydrate particles. Morphology studies of four experimental runs 2–5 from set S1 are presented in Figure 13. In runs 2 and 3, CO_2 + N_2 is injected, while in runs 4 and 5, CO_2 is injected. For all four cases, visual inspection suggests the presence of crystal morphology without any visible water. Set S1 includes IPR = 28 bars, which results in decomposition of methane hydrate into methane gas and water. Produced water converts back into hydrate in the presence of hydrate-forming gases CO_2 + N_2 and CO_2; however, in the presence of N_2, lower conversion of methane into methane hydrate occurs, which explains the higher methane-recovery efficiency in set S1. Morphology in runs 2 and 3 appear to be less dense compared to runs 4 and 5, which could be due to the presence of CH_4–CO_2 mixed hydrates in those runs. The difference in morphology is a direct indicator of CO_2 concentration available in injected gas. Higher CO_2 content in injected gas and higher content of CH_4–CO_2 mixed hydrates correspond to denser hydrates and lower methane recovery. Figure 14 showcases the morphology in runs 6–10 from set S2. In these runs, an IPR equal to 10 bars is applied below the methane hydrate stability pressure and CO_2 + N_2 is injected. In experimental run #6, 20% CO_2 is used, while in other cases, 10% CO_2 is used. In run #6, the presence of crystal morphology is recorded, while in other cases, hydrate slurry is recorded. In these runs, due to a small pressure reduction, methane hydrate goes into a metastable state and the presence of N_2 in CO_2 + N_2 acts as a driver for the complete dissociation of methane hydrate and the release of water. However, due to a lower concentration of CO_2, CH_4–CO_2 hydrate does not form and water production is observed. In experimental run #6, a higher CO_2 content creates enough driving force for CH_4–CO_2 hydrate formation and dissociated water to convert into CH_4–CO_2 mixed hydrate. Runs# 9 and 10 include the methane hydrate using SDS 2000 and 3000 ppm concentrations; however, presence of SDS and change in SDS concentration do not influence the risk of water production and hydrate morphology.

Figure 15 includes the morphology of the experimental runs 11–14 from set S2. In these runs, an IPR equal to 10 bars is applied, the pressure is reduced below the methane hydrate stability pressure, and pure CO_2 gas is injected. CO_2 injection leads to CH_4–CO_2 mixed hydrate formation. With the exception of run #12, we identify the morphology as crystalline for all runs. A reason for the presence of water in run #12 could be the presence of air while injecting CO_2 (hence the presence of N_2), which causes a lower driving force for hydrate to form. Comparing runs 2, 3, 7, and 8, it can be concluded that the degree of pressure reduction combined with CH_4–CO_2 exchange has little impact on mixed hydrate stability while keeping all other parameters constant.

Table 6. Results of the morphology study. Runs 1–5 are from set S1 and runs 6–14 are from set S2 (** for runs 9 and 10, methane hydrate is formed using 2000 ppm and 3000 ppm SDS solution, respectively). P_{inj} is the injection pressure of CO_2 rich gas and Pf is the mixed hydrate stability pressure at the end of run.

Run#	$P_{stability}$ (bars)	IPR (bars)	P_3 (bars)	Gas Type	P_{inj} (bars)	P_f (bars)	Morphology
1	28.50	ΔP = 28	0.3	CO_2 (10%) + N_2 (90%)	8.1	30.7	No picture
2	27.80	ΔP = 28	0.9	CO_2 (10%) + N_2 (90%)	20.9	30.5	Crystal
3	29.60	ΔP = 28	0.6	CO_2 (10%) + N_2 (90%)	30.6	43.8	Crystal
4	28.52	ΔP = 28	0.6	CO_2	43.1	37.9	Crystal
5	27.80	ΔP = 28	0.5	CO_2	39.2	37.3	Crystal
6	26.48	ΔP = 10	16.6	CO_2 (20%) + N_2 (90%)	29.06	25.00	Crystal
7	27.10	ΔP = 10	18.2	CO_2 (10%) + N_2 (90%)	21.55	26.20	Slurry
8	27.32	ΔP = 10	18.3	CO_2 (10%) + N_2 (90%)	30.42	34.59	Slurry
9 **	27.32	ΔP = 10	16.4	CO_2 (10%) + N_2 (90%)	29.10	30.80	Slurry
10 **	27.62	ΔP = 10	18.9	CO_2 (10%) + N_2 (90%)	29.40	34.30	Slurry
11	27.49	ΔP = 10	15.1	CO_2	30.20	22.00	Crystal
12	26.92	ΔP = 10	15.5	CO_2	21.19	18.70	Slurry
13	28.66	ΔP = 10	17.5	CO_2	30.09	23.17	Crystal
14	27.23	ΔP = 10	17.6	CO_2	27.41	21.76	Crystal

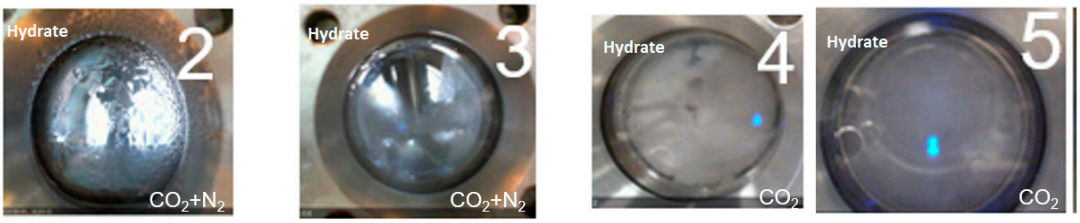

Figure 13. Hydrate morphology after gas injection when ΔP = 28 bars. Runs 2 and 3: CO_2 + N_2 injected; runs 4 and 5: CO_2 injected; run #1: No picture is available. Hydrate morphology is recorded at the end in every run.

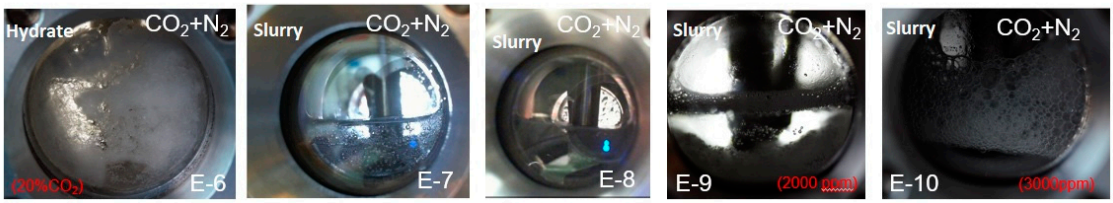

Figure 14. Hydrate morphology after CO_2 + N_2 gas injection when ΔP = 10 bars. Morphology at the end of the replacement reaction. Runs 6–10: CO + N_2 is injected; in Run #6: Hydrate crystal are observed while in Runs #7, 8, 9, 10, hydrate slurry is observed.

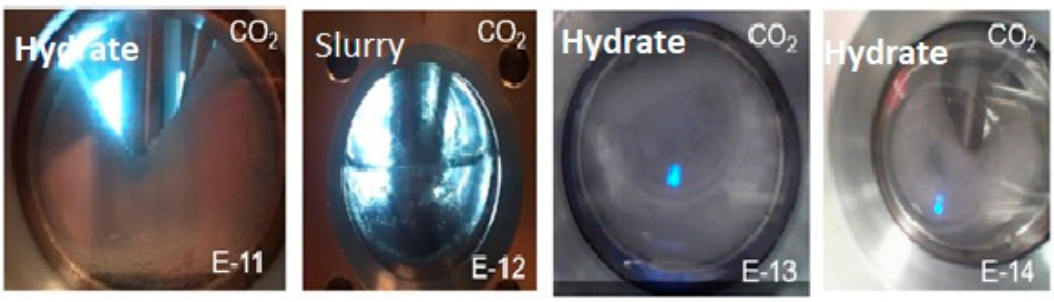

Figure 15. Hydrate morphology after CO_2 gas injection when ΔP = 10 bars. Morphology at the end of replacement reaction. Runs 11–15: CO_2 is injected; in Run#12: Hydrate slurry is observed while in Runs #11, 13, 14 hydrate crystals are observed.

In Figure 14 we see that in runs 7–10 in set S2, we injected CO_2 + N_2, and hydrate slurry formed, which includes the water and hydrate particle system. However, run #6, when CO_2 + N_2 with 20% CO_2 was injected and hydrate crystals formed at the end of replacement experiment. Figure 15 shows the morphology at the end of runs 11–14 from set S2. In these cases, CO_2 gas was injected. We observed water in run #12; runs 11, 13, and 15 showed hydrate crystal formation.

The overall conclusion from the morphology study is that water production using the combined method of pressure reduction followed by CO_2-rich gas injection using the huff-and-puff production technique is a stochastic phenomenon, which depends on many factors, including the degree of pressure reduction, type of gas injected, and composition of the gas injected. Water production risk is higher when injecting the CO_2 + N_2 gas, as shown in Figure 13. It can be explained as the role of N_2 in dissociating the methane hydrate and lowering the driving force of CO_2 + N_2 gas mixture compared with pure CO_2. This risk can be lowered further if the CO_2 concentration in the mixture is increased. Increasing the CO_2 percentage not only reduces the risk of water production, but it also makes the mixed hydrate more stable than the methane hydrate after replacement without affecting the methane recovery, as shown in Figures 10 and 14. A higher degree of pressure reduction could generate enough water, which might accelerate CH_4–CO_2 mixed hydrate formation and could reduce the risk of water production. However, the presence of N_2 in the environment might improve methane recovery, as previously discussed.

Morphology studies also suggest that mass-transfer improvement through pressure reduction is the dominating mechanism compared to the chemical method of improving mass transfer, as an increase in SDS concentration did not lead to a change in morphology (see runs 8, 9, and 10 in Table 5). Based on morphological evidence, we propose the hypothesis that the mechanism between CH_4–CO_2 exchanges includes CH_4-hydrate dissociation and release of free water converting back to CH_4–CO_2 mixed hydrates. Methane recovery ceases when free water is unavailable. Thus, it can be proposed that CH_4–CO_2 exchange includes methane hydrate dissociation and reconversion into CH_4-CO_2 mixed hydrate. This is the reason why a higher methane recovery is found for ΔP = 28 bars, whereas for ΔP = 10 bars, a lower methane recovery is observed. Initiating the controlled dissociation would allow us to produce a higher degree of methane while storing the CO_2. In the combined approach using the huff-and-puff production technique, controlled dissociation before the gas injection leads to a higher degree of methane recovery as well as a lower risk of water production, as our experimental results suggest.

4. Conclusions

Depressurization-assisted CH_4–CO_2 replacement is more promising technique than chemical-assisted CH_4–CO_2 replacement. Risk of water production in depressurization-assisted CH_4–CO_2 replacement depends on the degree of pressure reduction and type of gas injected. CH_4–CO_2 replacement includes two crucial considerations: Hydrate stability and gas recovery. Final selection of CO_2-rich gas during CH_4–CO_2 replacement is based on a tradeoff between hydrate stability and methane-recovery efficiency. A CO_2 + N_2 gas mixture is a good candidate for higher methane recovery and higher CO_2 concentration in CO_2 + N_2 mixture would lead to methane recovery and leave more stable mixed CH_4–CO_2 hydrates. Methane hydrate dissociation is the dominating mechanism to produce higher methane recovery and the pressure-assisted CH_4–CO_2 replacement in a controlled environment would lower the risk of water production and improve the methane recovery compared to only the depressurization method. Presence of the hydrate promoter SDS does not influence the CH_4–CO_2 exchange and does not have an effect on hydrate stability and methane recovery; however, it helps in reducing the uncertainty in methane hydrate formation and leads to similar initial conditions and shortens the experimental time.

Author Contributions: Conceptualization, investigation, original draft preparation, and review and editing: J.S.P.; supervision, project administration, and funding acquisition: N.v.S.

Funding: This research is funded by The Danish Council for Independent Research.

Conflicts of Interest: The authors declare no conflict of interest.

References

1. Sloan, E.D.; Koh, C.A.; Koh, C. *Clathrate Hydrates of Natural Gases*, 3rd ed.; CRC Press: Boca Raton, FL, USA, 2007.
2. Mu, L.; von Solms, N. Methane production and carbon capture by hydrate swapping. *Energy Fuels* **2017**, *31*, 3338–3347. [CrossRef]
3. Lee, J.D.; Susilo, R.; Englezos, P. Methane—Ethane and methane—Propane hydrate formation and decomposition on water droplets. *Chem. Eng. Sci.* **2005**, *60*, 4203–4212.
4. Yoon, J.; Kawamura, T.; Yamamoto, Y.; Komai, T. Transformation of methane hydrate to carbon dioxide hydrate: In situ raman spectroscopic observations. *J. Phys. Chem. A* **2004**, *108*, 5057–5059. [CrossRef]
5. Zhao, J.; Zhang, L.; Chen, X.; Fu, Z.; Liu, Y.; Song, Y. Experimental study of conditions for methane hydrate productivity by the CO_2 swap method. *Energy Fuels* **2015**, *29*, 6887–6895. [CrossRef]
6. McGrail, B.P.; Zhu, T.; Hunter, R.B.; White, M.D.; Patil, S.L.; Kulkarni, A.S. A new method for enhanced production of gas hydrates with CO_2. In Proceedings of the AAPG Hedberg Conference, Vancouver, BC, Canada, 12–16 September 2004; Volume 1, pp. 1–3.
7. Hauge, L.P.; Birkedal, K.A.; Ersland, G.; Graue, A. Methane production from natural gas hydrates by CO_2 replacement—Review of lab experiments and field trial. In Proceedings of the SPE Conference, Bergen, Norway, 2 April 2014.
8. Zhou, X.; Fan, S.; Liang, D.; Du, J. Replacement of methane from quartz sand-bearing hydrate with carbon dioxide-in-water emulsion. *Energy Fuels* **2008**, *22*, 1759–1764. [CrossRef]
9. Kang, S.; Lee, J. Kinetic behaviors of CO_2 hydrates in porous media and effect of kinetic promoter on the formation kinetics. *Chem. Eng. Sci.* **2010**, *65*, 1840–1845. [CrossRef]
10. Huang, D.; Fan, S. Thermal conductivity of methane hydrate formed from sodium dodecyl sulfate solution. *J. Chem. Eng. Data* **2004**, *49*, 1479–1482. [CrossRef]
11. Choudhary, N.; Hande, V.R.; Roy, S.; Chakrabarty, S.; Kumar, R. Effect of sodium dodecyl sulfate surfactant on methane hydrate formation: A molecular dynamics study. *J. Phys. Chem. B* **2018**, *122*, 6536–6542. [CrossRef]
12. Kumar, A.; Bhattacharjee, G.; Kulkarni, B.D.; Kumar, R. Role of surfactants in promoting gas hydrate formation. *Ind. Eng. Chem. Res.* **2015**, *54*, 12217–12232. [CrossRef]
13. Bhattacharjee, G.; Sangwai, J.S.; Veluswamy, H.P.; Kumar, R.; Linga, P.; Pandey, G. Alleviation of Foam Formation in a Surfactant Driven Gas Hydrate System: Insights via a Detailed Morphological Study. *ACS Appl. Energy Mater.* **2018**, *1*, 6899–6911.
14. Liu, P.; Chen, J.; Wang, X.; Ma, Q.; Sun, C.; Yang, L.; Tang, X.; Chen, G. The specific surface area of methane hydrate formed in different conditions and manners. *Sci. China Ser. B Chem.* **2009**, *52*, 381–386.
15. Zhou, X.; Fan, S.; Liang, D.; Du, J. Determination of appropriate condition on replacing methane from hydrate with carbon dioxide. *Energy Convers. Manag.* **2008**, *49*, 2124–2129. [CrossRef]
16. Jensen, L.; Thomsen, K.; von Solms, N. Propane hydrate nucleation: Experimental investigation and correlation. *Chem. Eng. Sci.* **2008**, *63*, 3069–3080. [CrossRef]
17. Zhao, J.; Xu, K.; Song, Y.; Liu, W.; Lam, W.; Liu, Y.; Xue, K.; Zhu, Y.; Yu, X.; Li, Q. A Review on Research on Replacement of CH4 in Natural Gas Hydrates by Use of CO_2. *Energies* **2012**, *5*, 399–419. [CrossRef]
18. Chong, Z.R.; Yang, S.H.B.; Babu, P.; Linga, P.; Li, X. Sen Review of natural gas hydrates as an energy resource: Prospects and challenges. *Appl. Energy* **2016**, *162*, 1633–1652. [CrossRef]
19. Dashti, H.; Yew, L.Z.; Lou, X. Recent advances in gas hydrate-based CO_2 capture.pdf. *J. Nat. Gas Sci. Eng.* **2015**, *23*, 195–207. [CrossRef]
20. Komatsu, H.; Ota, M.; Smith, R.L.; Inomata, H. Review of CO_2-CH_4 clathrate hydrate replacement reaction laboratory studies—Properties and kinetics. *J. Taiwan Inst. Chem. Eng.* **2013**, *44*, 517–537. [CrossRef]
21. Castellani, B.; Rossetti, G.; Tupsakhare, S.; Rossi, F.; Nicolini, A.; Castaldi, M.J. Simulation of CO_2 storage and methane gas production from gas hydrates in a large scale laboratory reactor. *J. Pet. Sci. Eng.* **2016**, *147*, 515–527. [CrossRef]

22. Tupsakhare, S.S.; Castaldi, M.J. Efficiency enhancements in methane recovery from natural gas hydrates using injection of CO_2/N_2 gas mixture simulating in-situ combustion. *Appl. Energy* **2019**, *236*, 825–836. [CrossRef]
23. Zhao, J.; Zhang, L.; Chen, X.; Zhang, Y.; Liu, Y.; Song, Y. Combined replacement and depressurization methane hydrate recovery method. *Energy Explor. Exploit.* **2016**, *34*, 129–139. [CrossRef]
24. Li, S.; Zheng, R.; Xu, X.; Hou, J. Energy efficiency analysis of hydrate dissociation by thermal stimulation. *J. Nat. Gas Sci. Eng.* **2016**, *30*, 148–155. [CrossRef]
25. Circone, S.; Kirby, S.H.; Stern, L.A. Direct measurement of methane hydrate composition along the hydrate equilibrium boundary. *J. Phys. Chem. B* **2005**, *109*, 9468–9475. [CrossRef] [PubMed]
26. Jia, B.; Tsau, J.S.; Barati, R. A review of the current progress of CO_2 injection EOR and carbon storage in shale oil reservoirs. *Fuel* **2019**, *236*, 404–427. [CrossRef]
27. Ke, W.; Svartaas, T.M.; Chen, D. A review of gas hydrate nucleation theories and growth models. *J. Nat. Gas Sci. Eng.* **2018**, *61*, 169–196. [CrossRef]
28. Ganji, H.; Manteghian, M.; Sadaghiani, K.; Omidkhah, M.R.; Mofrad, H.R. Effect of different surfactants on methane hydrate formation rate, stability and storage capacity. *Fuel* **2007**, *86*, 434–441. [CrossRef]
29. Linga, P.; Clarke, M.A. A review of reactor designs and materials employed for increasing the rate of gas hydrate formation. *Energy Fuels* **2017**, *31*, 1–13. [CrossRef]
30. Tsypkin, G.G. Thermodynamic conditions of formation of CO_2 hydrate in carbon dioxide injection into a methane hydrate reservoir. *Fluid Dyn.* **2018**, *53*, 680–689. [CrossRef]
31. Koh, D.Y.; Kang, H.; Lee, J.W.; Park, Y.; Kim, S.J.; Lee, J.; Lee, J.Y.; Lee, H. Energy-efficient natural gas hydrate production using gas exchange. *Appl. Energy* **2016**, *162*, 114–130. [CrossRef]
32. Chen, Y.; Gao, Y.; Zhao, Y.; Chen, L.; Dong, C.; Sun, B. Experimental investigation of different factors in fluencing the replacement efficiency of CO_2 for methane hydrate. *Appl. Energy* **2018**, *228*, 309–316. [CrossRef]